ISBN: 978-3-95450-231-8 ISSN: 2673-5490 doi: 10.18429/JACoW-IPAC2023-WEPA088

SCATTERED FIELD FORMULATION FOR WAKEFIELD AND SPACE CHARGE CALCULATIONS*

J. Christ†, E. Gjonaj
Institute for Accelerator Science and Electromagnetic Fields (TEMF), Darmstadt, Germany

Abstract

In the injector section of electron linacs, both internal space charge forces and wakefield effects influence the beam dynamics. The common distinction between particle tracking codes in the bunch reference frame and wakefield codes does not allow to consider both effects simultaneously. We propose a scattered field formulation that takes into account the coupled effects of space charge and wakefield interactions, respectively. This approach is applied in the simulation of wakefields and the beam dynamics for an RF-photogun prototype with retracted cathode that is intended for use in the European XFEL. The influence of the wakefields originating from the retracted cathode structure is investigated.

INTRODUCTION

The design and optimization of FEL light sources require detailed knowledge of the beam dynamics in the injector section. In the electron gun, internal space charge forces and externally applied fields are the dominant contributions to the beam dynamics. Hence, simulations typically focus on these effects, neglecting transient electromagnetic wakefields arising from the interaction with the walls or synchrotron radiation. Due to the low energy of the bunch immediately after emission, however, wakefields may contribute to additional energy spread and emittance growth.

In this paper, we present a methodology used to combine wakefield and space charge calculations. In the following, we first describe the basic procedures and codes used for space charge and wakefield calculations, respectively. Then, the coupling procedure applying a scattered field formulation is described. The method is applied in the simulation of a prototype of an electron gun with retracted cathode for the European XFEL. Results of first numerical studies for this device are presented. Throughout the paper the term wakefield is used interchangeably for the HF fields caused by the passage of the bunch through a chamber.

METHOD

Wakefield Computation with PBCI

The coupling procedure uses a fork of the in-house wakefield code *Parallel Beam Cavity Interaction* (PBCI) [1]. It is based on the 3D time domain Finite Integration Technique (FIT) discretization of electric and magnetic fields which leads to the semi-discrete system of equations [2]

$$\frac{\mathrm{d}}{\mathrm{d}t}\begin{pmatrix}\widehat{\mathbf{e}}\\ \widehat{\mathbf{h}}\end{pmatrix} = \begin{pmatrix}0 & \mathbf{M}_{\varepsilon}^{-1}\mathbf{C}^{T}\\ -\mathbf{M}_{\mu}^{-1}\mathbf{C} & 0\end{pmatrix}\begin{pmatrix}\widehat{\mathbf{e}}\\ \widehat{\mathbf{h}}\end{pmatrix} - \begin{pmatrix}\mathbf{M}_{\varepsilon}^{-1}\widehat{\widehat{\mathbf{j}}}\\ 0\end{pmatrix} \quad (1)$$

with $\widehat{\mathbf{e}}$ and $\widehat{\mathbf{h}}$ describing electric and magnetic voltages in a staggered, cartesian grid. The topological curl matrix $\mathbf{C}$ and the diagonal material matrices $\mathbf{M}_{\mu}^{-1}$ and $\mathbf{M}_{\varepsilon}^{-1}$ denote discretization matrices on the grid whereas the current excitation is given by $\widehat{\widehat{\mathbf{j}}}$. Perfectly conducting (PEC) materials are accounted for by imposing vanishing electric fields at the boundaries. For a better approximation of curved boundaries, a conformal boundary approximation is applied that enables 2nd order accuracy for arbitrary geometries [3, 4].

In PBCI, the time discretization is realized by means of a directional operator splitting method which is strictly dispersion-free for longitudinal wave propagation. A moving window mesh as well as multi-node and multi-thread parallelization are used to improve performance, to name just some of the features relevant for this work [1].

Particle Tracking with REPTIL

For the computation of beam dynamics with space charge fields, the particle tracking code *Relativistic Particle Tracker for Injectors and Linacs* (REPTIL) is employed [5]. The code iterates between an update of the particle's equations of motion and the solution of the electrostatic problem in the rest frame of the bunch, providing an instantaneous electromagnetic field in the laboratory frame. For the free-space field solution in the rest frame, REPTIL provides a Green-function solver based on 3D Discrete Fourier Transforms as well as various particle-particle solvers. In particular, the Fast-Multipole Method (FMM) will be used in the following to enable the coupling of the intrinsic space charge fields of the beam to geometrical wakefields. The particle positions and momenta are updated with a RK-4 time integrator.

Scattered Field Formulation

In the scattered field formulation, the total electric field $\mathbf{E}_{\mathrm{t}}$ is decomposed into a scattered and an incident field,

$$\mathbf{E}_{\mathrm{t}} = \mathbf{E}_{\mathrm{s}} + \mathbf{E}_{\mathrm{i}}, \quad (2)$$

and accordingly for the magnetic field. The incident field, $\mathbf{E}_{\mathrm{i}}$, satisfies Maxwell's equations for the given current density subject to arbitrary (but wisely chosen) boundary conditions. Thus, to fulfill the physical boundary conditions for the total field appropriate boundary conditions must be imposed on the scattered field $\mathbf{E}_{\mathrm{s}}$. For the problem under consideration, the incident field is given by the particle tracker REPTIL

* Work funded by the Deutsche Forschungsgemeinschaft (DFG, German Research Foundation) – Project-ID 264883531 – GRK 2128 "AccelencE"
† jonas.christ@tu-darmstadt.de

ISBN: 978-3-95450-231-8 ISSN: 2673-5490 doi: 10.18429/JACoW-IPAC2023-WEPA088

providing the space charge field generated by the bunch using (unphysical) free space boundary conditions. Therefore, the scattered field represents a solution of the source-free Maxwell equations with non-trivial boundary conditions compensating for the unphysical incident field at the boundary. On a PEC surface with normal vector $\mathbf{n}$, the scattered field has to fulfill

$$\mathbf{n} \times \mathbf{E}_\mathrm{s}|_\mathrm{PEC} = -\mathbf{n} \times \mathbf{E}_\mathrm{i}|_\mathrm{PEC}. \tag{3}$$

Equation (3) may be directly imposed by fixing the degrees of freedom on the PEC surface before solving for the remaining unknowns. However, we propose a different approach that is less intrusive on the update equations. Figure 1 displays an exemplary single primal face on the grid, interfacing a straight PEC-boundary. The semi-discrete Faraday's law in FIT notation for this face reads

$$\frac{\mathrm{d}}{\mathrm{d}t}\widehat{\mathbf{h}}_k = -[\mathbf{M}_\mu^{-1}]_{kk}\left(\sum_j [\mathbf{C}]_{kj}\widehat{\mathbf{e}}_j - \widehat{\mathbf{e}}_\mathrm{tan}\right), \tag{4}$$

where $\widehat{\mathbf{e}}_\mathrm{tan}$ is the voltage along the PEC edge obtained by Eq. (3) and $\widehat{\mathbf{e}}_j$ are the voltages of the scattered field $\mathbf{E}_\mathrm{s}$ on the face edges. Note that therefore, the scattered field does not need to be computed on the PEC edges. Given a discretization of the incident field $\mathbf{E}_\mathrm{i}$ on the same grid, $\widehat{\mathbf{e}}_\mathrm{tan}$ is readily found to

$$\widehat{\mathbf{e}}_\mathrm{tan} = \sum_j [\mathbf{I}]_{jj}\widehat{\mathbf{e}}_{\mathrm{i},j} \tag{5}$$

with $[\mathbf{I}]_{jj} = -1$ if the edge j is part of PEC and 0 otherwise. The resulting semi-discrete system of Maxwell equations on the grid for the scattered field is

$$\frac{\mathrm{d}}{\mathrm{d}t}\begin{pmatrix}\widehat{\mathbf{e}}\\ \widehat{\mathbf{h}}\end{pmatrix} = \begin{pmatrix}0 & \mathbf{M}_\varepsilon^{-1}\mathbf{C}^T\\ -\mathbf{M}_\mu^{-1}\mathbf{C} & 0\end{pmatrix}\begin{pmatrix}\widehat{\mathbf{e}}\\ \widehat{\mathbf{h}}\end{pmatrix} - \begin{pmatrix}0\\ \mathbf{M}_\mu^{-1}\mathbf{C}\mathbf{I}\widehat{\mathbf{e}}_\mathrm{i}\end{pmatrix}. \tag{6}$$

The degrees of freedom now describe only the scattered field whereas the incident field gives rise to a magnetic-type current at the boundary that serves as an excitation. The discretization matrices of the FIT-method remain the same as in Eq. (1).

The above procedure for the computation of $\widehat{\mathbf{e}}_\mathrm{tan}$ can be generalized for a conformal boundary approximation, resulting in a non-diagonal interpolation matrix $\mathbf{I}$ (not discussed in this paper). To compute $\widehat{\mathbf{e}}_\mathrm{i}$, the evaluation of the space charge field on the FIT grid nodes is needed. Since the non-zero entries of $\mathbf{I}$ are known, this evaluation is not necessary in the whole computational domain. For this purpose, it is sufficient to evaluate the incident field only in the vicinity of PEC surfaces. Furthermore, given the different length scales of geometry and particle bunch, the evaluation of space charge fields on a large grid enclosing the geometry is numerically not feasible. Instead, the FMM implemented in REPTIL is used to obtain the incident field only at the relevant boundary nodes from the individual particles in the bunch distribution [6].

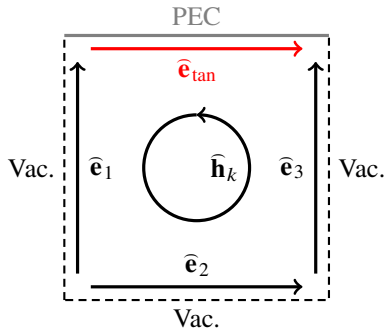

Figure 1: Primal FIT face with PEC edge, depicting the allocation of field components at a PEC boundary.

RESULTS

The model under investigation is a superconducting 1.6-cell TESLA-type RF-gun with a retractable cathode plug as shown in Fig. 2. This gun design is the preferred solution for the future upgrade of the European XFEL to support a future high duty cycle operation mode [7]. In the following, the cathode plug is retracted by 0.45 mm with respect to the cavity back wall. Using commercial software, the field modes and resulting field along the axis are found for the cavity geometry [8]. In Ref. [7], a multiobjective optimization procedure is used to determine the optimal gun parameters including the RF-phase, solenoid setup, the laser spot size and its duration for a 100 pC bunch. The reader is referred to Ref. [7] for a description of these parameters.

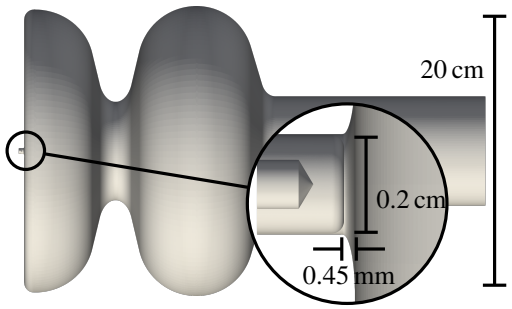

Figure 2: RF-gun model used in the simulations, highlighting the retraction of the cathode with respect to the backplane.

The beam evolves under the effect of space charge and external fields only. The effect of wakefields is not considered in the particle tracking. The resulting scattered field distribution for different bunch positions is presented in Fig. 3. It can clearly be seen how wakefields start from the cathode plug, the iris and the transition to the beam pipe.

To determine the influence of the wakefields on the bunch, the momentum change caused by the wave fields on a single particle n at position $\mathbf{r}_n\,(t)$ with velocity $\mathbf{v}_n\,(t)$,

$$\Delta\mathbf{p}_n\,(t) = q_n \int_0^t \mathbf{E}_\mathrm{s}\,(\mathbf{r}_n, t) + \mathbf{v}_n \times \mathbf{B}_\mathrm{s}\,(\mathbf{r}_n, t)\,\mathrm{d}t \tag{7}$$

is computed.

ISBN: 978-3-95450-231-8 ISSN: 2673-5490 doi: 10.18429/JACoW-IPAC2023-WEPA088

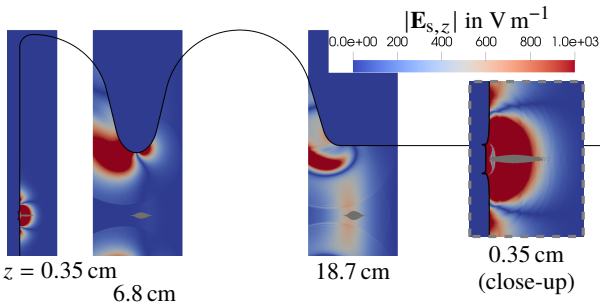

Figure 3: Scattered wakefields within the moving computational window at different bunch positions. The bunch is indicated in gray.

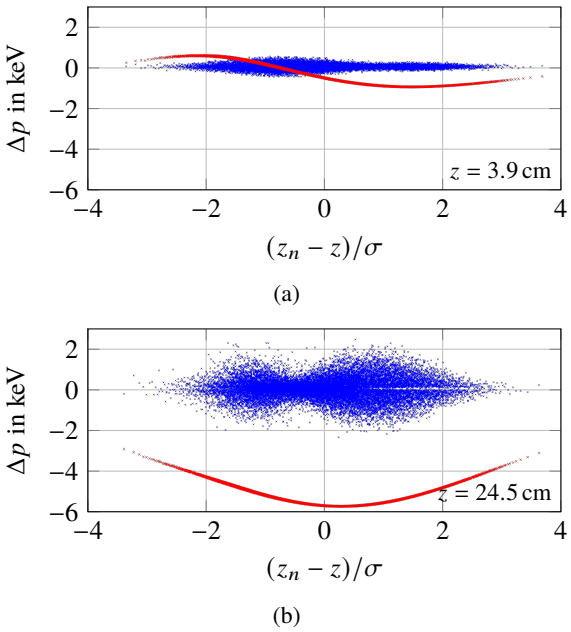

Figure 4: Distribution of momentum kicks $\Delta p_{y,n}$ (blue) and $\Delta p_{z,n}$ (red) due to the wakefields at two different bunch positions.

The impact of the wakefields on beam properties can be estimated from the momentum kicks received by the particles according to Eq. (7). For two exemplary bunch positions, the resulting distributions for $\Delta p_{y,n}$ and $\Delta p_{z,n}$ are shown in Fig. 4. At the first bunch position, only the wakefields from the retraction have reached the bunch. It can be seen that leading particles get slightly decelerated while trailing particles receive accelerating kicks, indicating that the retraction could improve the longitudinal energy spread. Transverse and longitudinal kicks are of similar order of magnitude. At the second bunch position, the longitudinal momentum change is significantly larger but more uniform than before, indicating that the impact of the scattered field from the iris and the transition is stronger than that of the cathode plug. Additionally, the transverse momentum change shows substantial increase as well.

The resulting deviations in both core slice energy spread (SES) and transverse emittance are depicted in Fig. 5. The transverse emittance is significantly increased over most of the bunch passage. The SES reduction is less than 4 % for any bunch position. These results show that the wakefields in the gun may have a significant impact on the beam emittance. However, for a conclusive result further beam dynamics and wakefield studies downstream of the remaining injector line are needed. The impact of the wakefields on the energy spread appears to be low. In particular, the influence of the cathode plug geometry is negligible.

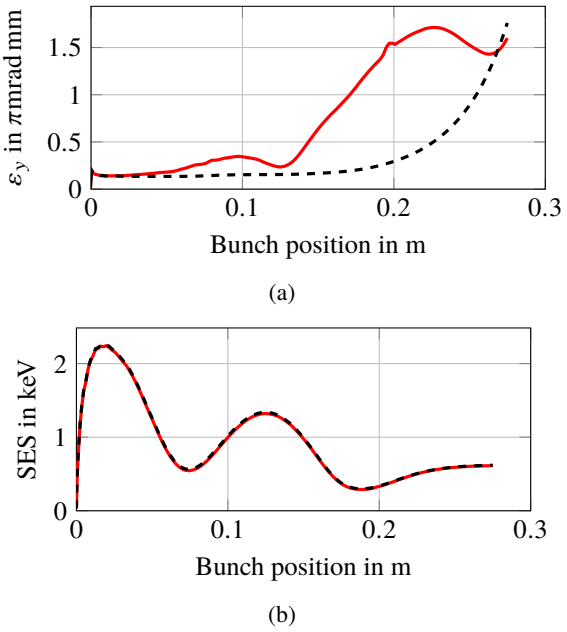

Figure 5: Transverse emittance (a) and energy spread (b) in the core slice with (red) and without (black) wakefields. The reduction in energy spread due to the wakefield is < 4 %.

CONCLUSION

For the prototype under investigation, we find significant impact of the wakefields on the beam emittance. The energy spread remains largely unaffected. The wakefield contributions are due mainly to the gun iris and the beam pipe transition rather than to the cathode plug introduced in the new European XFEL gun design. Further simulations downstream of the injector line are needed to fully asses the impact of the wakefields on the beam dynamics.

ACKNOWLEDGEMENTS

The authors would like to thank Dmitry Bazyl of Deutsches Elektronen-Synchrotron (DESY) for geometry and beam parameters of the gun model.

REFERENCES

[1] E. Gjonaj *et al.*, "Large Scale Parallel Wake Field Computations for 3D-Accelerator Structures with the PBCI Code," in *Proc. ICAP'06*, Chamonix, Switzerland, Oct. 2006, pp. 29–34. https://jacow.org/icap06/papers/MOM2IS02.pdf

ISBN: 978-3-95450-231-8 ISSN: 2673-5490 doi: 10.18429/JACoW-IPAC2023-WEPA088

[2] T. Weiland, "A Discretization Method for the Solution of Maxwell's Equations for Six-Component Fields," *AEU - International Journal of Electronics and Communications*, no. 31.3, pp. 116–120, 1977.

[3] S. Dey and R. Mittra, "A locally conformal finite-difference time-domain (FDTD) algorithm for modeling three-dimensional perfectly conducting objects," *IEEE Microwave and Guided Wave Letters*, vol. 7, no. 9, pp. 273–275, 1997. doi:10.1109/75.622536

[4] B. Krietenstein, R. Schuhmann, P. Thoma, and T. Weiland, "The Perfect Boundary Approximation Technique Facing the Big Challenge of High Precision Field Computation," in *Proc. LINAC'98*, Chicago, IL, USA, Aug. 1998, pp. 860–862. https://jacow.org/l98/papers/TH4041.pdf

[5] E. Gjonaj, *REPTIL – Status of development and overview of capabilities*, 2022. https://www.desy.de/xfel-beam/s2e/talks/2022_01_11/EG.pdf

[6] S. A. Schmid, H. D. Gersem, M. Dohlus, and E. Gjonaj, "Simulating Space Charge Dominated Beam Dynamics Using FMM," in *Proc. NAPAC'19*, Lansing, MI, USA, Sep. 2019, pp. 909–911. doi:10.18429/JACoW-NAPAC2019-WEPLE10

[7] H. Vennekate, A. Arnold, P. Lu, P. Murcek, J. Teichert, and R. Xiang, "Emittance compensation schemes for a superconducting rf injector," *Physical Review Accelerators and Beams*, vol. 21, no. 9, 2018. doi:10.1103/PhysRevAccelBeams.21.093403

[8] Dassault Systems, *CST Studio Suite*, 2022. https://www.3ds.com